ELSEVIER

Contents lists available at ScienceDirect

### International Journal of Pharmaceutics

journal homepage: www.elsevier.com/locate/ijpharm





# Optimizing mRNA delivery: A microfluidic exploration of DOTMA vs. DOTAP lipid nanoparticles for GFP expression on human PBMCs and THP-1 cell line

Erwin Pavel Lamparelli <sup>a</sup>, Elena Ciaglia <sup>a,c</sup>, Maria Camilla Ciardulli <sup>b</sup>, Valentina Lopardo <sup>a</sup>, Francesco Montella <sup>a</sup>, Alessandro Annibale Puca <sup>a,c</sup>, Giovanna Della Porta <sup>a,d,\*</sup>

- <sup>a</sup> Department of Medicine, Surgery and Dentistry, University of Salerno, Via S. Allende, Baronissi, SA 84081, Italy
- b Department of Biomaterials and Biomedical Technology, University Medical Center Groningen, A. Deusinglaan 1, Groningen 9713 AV, the Netherlands
- <sup>c</sup> Cardiovascular Research Unit, IRCCS MultiMedica, Milan 20138, Italy
- d Interdepartment Centre BIONAM, Università di Salerno, via Giovanni Paolo I, Fisciano, SA 84084, Italy

### ARTICLE INFO

### Keywords: mRNA-eGFP delivery Microfluidic technology Lipid Nanoparticles Cationic lipids Human PBMCs THP-1 cell line

### ABSTRACT

This study highlights lipid nanoparticle (LNP) formulations incorporating DOTMA or DOTAP as cationic lipids for the delivery of mRNA encoding Enhanced Green Fluorescent Protein (eGFP-mRNA). The performance of these tailored formulations was benchmarked against a commercial formulation (LipidFlex), Precigenome), which can also be combined with DOTMA or DOTAP but contains helper lipids of undisclosed composition. LNPs were synthesized using a microfluidic device equipped with a passive Y-shaped microchip, operating at an optimized total flow rate of 6 mL/min and a flow rate ratio of 1:3, with a total lipid concentration ranging from 0.7 to 30 mM. This method produced Single~Unilamellar~Vesicles~(SUVs) with an average size of  $150\pm53$  nm and a surface charge of 18 mV. The nitrogen-to-phosphate (N/P) ratio was varied between 250 and 6, modulating the surface charge (from 48 to 18 mV) and the mRNA-eGFP encapsulation efficiency (from 80 % to 70 %, respectively). Cytotoxicity assays and IC $_{50}$  evaluations on a Hamster Ovarian cell line confirmed that the c-DOTMA formulation achieved an optimal balance of low toxicity and high transfection efficiency. In THP-1 cells, c-DOTMA delivered the highest eGFP expression, reaching up to 25 % transfection efficiency, extremely higher if compared to those observed in the total PBMC population under similar conditions. This selective behavior highlights its potential for precise mRNA delivery to specific immune cell subsets, though further research is required to assess in vivo performance, biodistribution, and immunogenicity.

### 1. Introduction

mRNA offers a significant advantage in gene delivery by enabling direct translation within the cell's cytoplasm. This process results in highly efficient transfection, as the mRNA bypasses the need for nuclear entry and integration into the host genome (Zhang et al., 2024). Unlike viral vectors, which carry the risk of random insertion into the genome and potential disruption of host cell functions, mRNA remains episomal, minimizing the risk of genomic mutations or undesired cellular effects (Ay and Reinisch, 2024).

This unique feature makes mRNA an attractive and safer option for therapeutic applications, including vaccines and gene therapies. However, the inherent instability of nucleic acids presents a significant challenge in mRNA delivery, as they are prone to degradation by enzymes and environmental factors (Zhang et al., 2023). This necessitates the development of advanced nanoparticle formulations that can protect mRNA molecules, ensuring their stability and facilitating efficient transport into target cells. Innovative nano-carriers, such as lipid nanoparticles (LNPs), offer promising solutions by encapsulating mRNA and shielding it from degradation while improving cellular uptake and release. The exploration of these robust delivery systems is crucial for enhancing the effectiveness of mRNA-based therapeutics and ensuring their safe and reliable delivery to specific target cells (Qin et al., 2022).

LNPs can be formulated with various lipid components, mainly cationic or ionizable lipids, which are crucial components for mRNA binding. Cationic lipids carry a permanent positive charge at

<sup>\*</sup> Corresponding author at: Department of Medicine, Surgery and Dentistry, University of Salerno, Via S. Allende, Baronissi, SA 84081, Italy. E-mail address: gdellaporta@unisa.it (G. Della Porta).

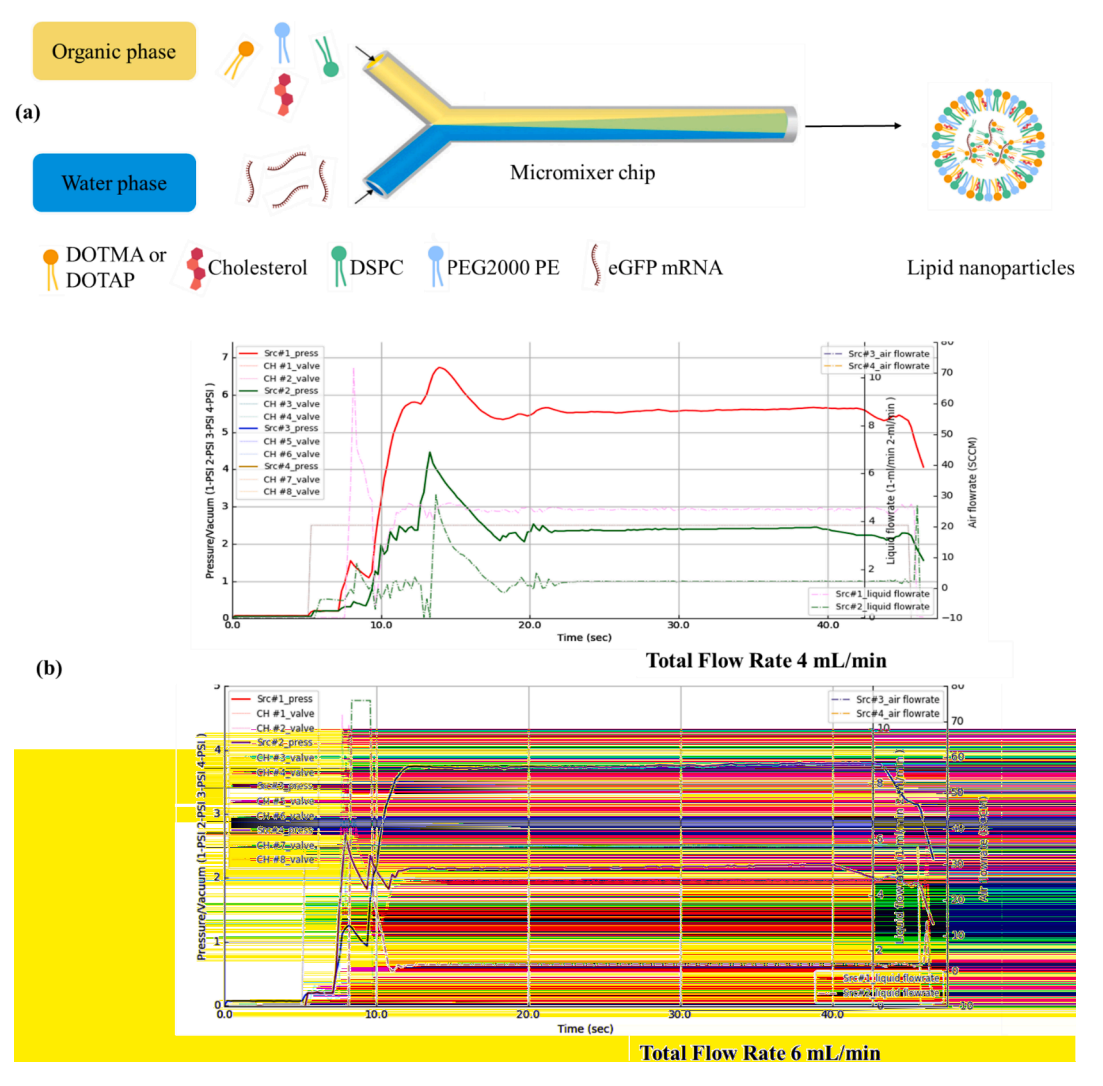


Fig. 1. Microfluidic Process schematic representation and Total Flow Rate (TFR) pressure diagrams. The illustration depicts a streamlined microfluidic setup for the ethanol injection method in lipid nanoparticle (LNP) synthesis. The key components include Inlet Channels for lipid solution inlets and aqueous solution. Microfluidic Mixing Junction adopted in present work is Y-shaped. (a). The diagrams indicated the measured pressure values vs. run time, illustrating the pressure behavior along the mixing process. A steady-state flow with constant pressure within the chip is more easily reached when operating at TFR of 6 mL/min; in this condition homogeneus mixing is achieved with uniform production of LNPs (b).

physiological pH, enabling strong electrostatic interactions with mRNA's negatively charged phosphate backbone (Guéguen et al., 2024). This property makes them effective in forming lipid-mRNA complexes to protect mRNA from enzymatic degradation and promote cellular uptake by facilitating endosomal escape through membrane destabilization (Pfeifer et al., 2023). Common examples include DOTMA (dimethyldioctadecylammonium) and DOTAP (1,2-dioleoyl-3-trimethylammonium-propane), which are widely used for their ability to interact with nucleic acids and enhance transfection efficiency. Their positive charge simplifies the formulation assembly, even if it can trigger immune responses or provoke inflammatory reactions, mainly when delivered over extended periods (Yew and Scheule, 2005).

Ionizable lipids are neutral at physiological pH but become positively charged in the acidic environment of the endosome; this behavior allows mRNA encapsulation and release in targeted conditions. Similar to cationic lipids, they destabilize the endosomal membrane, promoting mRNA release into the cytoplasm and showing reduced cytotoxic effects. However, their formulation requires a precise pH-sensitive design to achieve the desired charge-switching properties. Additionally, formulations with ionizable lipids may be less stable than cationic lipids, necessitating additional stabilization strategies (Swetha et al., 2023).

Other helper lipids in the formulation are neutral; such as DSPC (1,2-

distearoyl-sn-glycero-3-phosphocholine) and cholesterol, both included to stabilize the LNP structure and provide membrane rigidity with reduced toxicity. Cholesterol also helps maintain the integrity of the lipid bilayer, ensuring that the nanoparticles remain stable during storage and in vivo circulation. To further improve lipid carrier stability through steric interactions and prolong *in-vivo* half-life, PEG-based lipids are also included in formulations (Tenchov et al., 2023). Indeed, the PEG chains on the carrier surface reduce recognition and uptake by the immune system, leading to an increased circulation time in the body, improving the chances of reaching target cells and exerting therapeutic effects (Korzun et al., 2023).

Despite the extensive literature on formulation strategies, there is still a need for enhanced targeting of specific cell types, minimizing off-target effects, and improving tissue-specific delivery (Yin et al., 2023). This raises the need for better control over the formulation parameters, and cationic lipid formulations hold tremendous potential, enhancing delivery efficiency and ensuring an acceptable safety profile. Thus, although ionizable lipids are often preferred, formulations utilizing stable cationic lipids can be more effective in safely binding and delivering RNA. Additionally, formulations with cationic lipids frequently achieve a precise intracellular delivery and successfully address challenges, such as endosomal escape and RNA degradation, before reaching

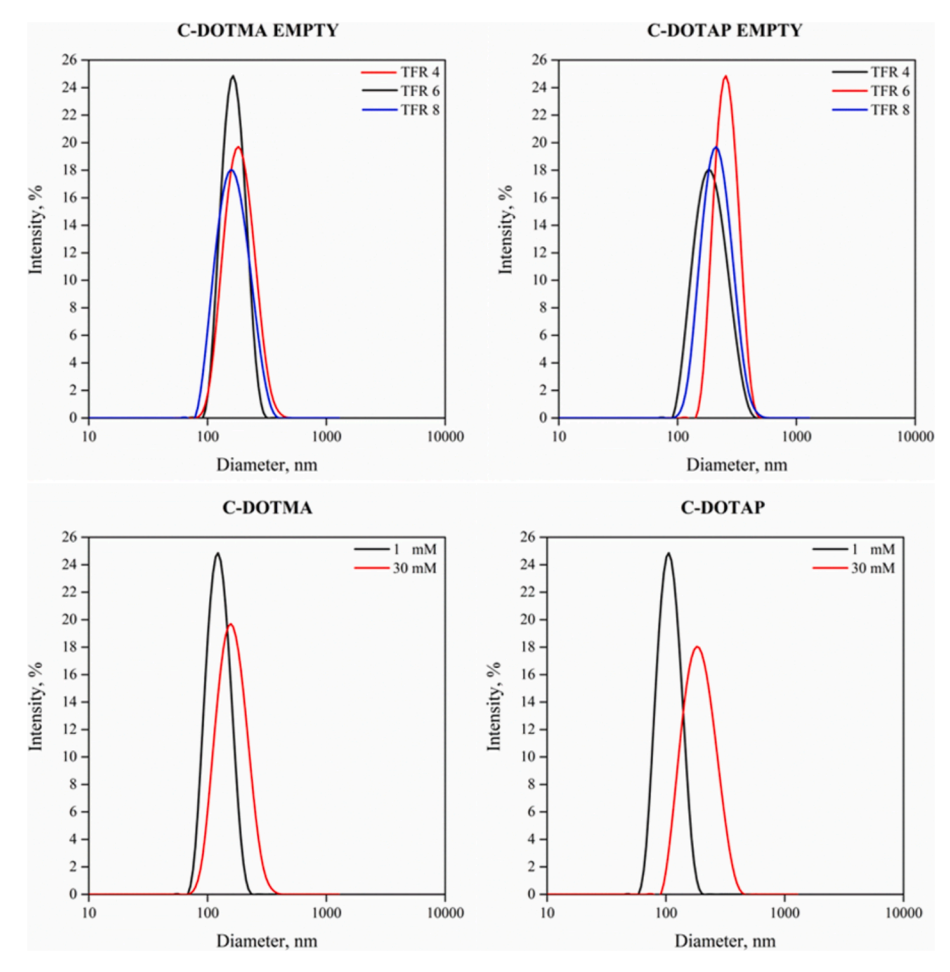


Fig. 2. Evaluation of microfluidic parameters and lipid concentration effect on LNP size and distributions. An increase in the Total Flow Rate (TFR) resulted in slightly broader LNP size distributions. Variations in Total Lipid Concentration from 1 to 30 mM, operating at fixed TFR of 6 mL/min, showed a direct correlation with LNPs size as higher lipid concentrations led to larger mean size and distribution.

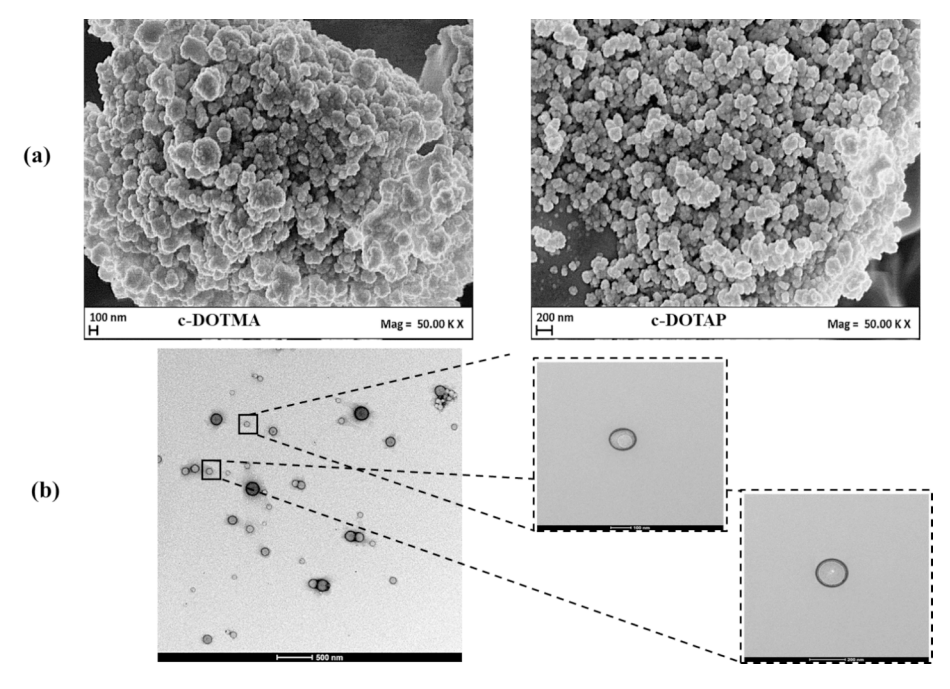


Fig. 3. Morphology and structure evaluation of customized formulation by Scanning and Transmission Electron microscopy. SEM micrographs revealed a spherical shape with highly uniform morphology. The vesicle agglomeration observed was primarily attributed to the drying process during sample preparation (a). TEM imaging confirmed the LNPs structure as Single Unilamellar Vesicle (SUV), clearly highlighted by the staining of the lipid membrane (b).

Table 1 Summary of all formulations evaluated, detailing the corresponding process parameters and characterization metrics. Data includes variations in Total Lipid Concentration (mM) in the oily phase adopted for microfluidic process; Total Flow Rate (TFR) along the process, LNPs Mean Size (MS, nm) and polydispersity index (PDI), assessments of  $\zeta$ -potential (Zp, mV), encapsulation efficiency (EE, %), nitrogen-to-phosphate ratio (N/P), IC<sub>50</sub> value at 24 h and transfection efficiency at 24 h (TE, %) on CHO-K1 cell line. Legend: c-, customized, LF: *LipidFlex* commercial mix; nd: not detected.

Formulations		mM	TFR	MS ± SD nm	PDI	ζp mV	IC <sub>50</sub> SLN/mL	EE,%	N/P ratio	TE %
Commercial	LF-DOTAP	30	6	$136 \pm 51$	0.14	52 ± 8	$1 \times 10^{11}$		_	_
	LF-DOTAP	30	6	$140\pm51$	0.13	$52\pm 8$	$7\times10^{10}$	$36\pm2$	6	38
	LF-DOTAP	30	6	$140\pm51$	0.13	$52\pm 8$	$8\times10^{10}$	$35\pm2$	230	1
	LF-DOTMA	30	6	$171\pm67$	0.15	$46 \pm 5$	$1\times10^{11}$		_	_
	LF-DOTMA	30	6	$175\pm60$	0.17	$47 \pm 7$	$7  imes 10^{10}$	$25\pm3$	6	70
	LF-DOTMA	30	6	$165 \pm 69$	0.17	$47 \pm 7$	$8  imes 10^{10}$	$95\pm1$	240	2
Customized	c-DOTAP	30	4	$189 \pm 75$	0.16	$45 \pm 7$			_	
	c-DOTAP	30	6	$220\pm89$	0.15	$24\pm7$	$2 \times 10^{10}$		_	
	c-DOTAP	30	8	$223 \pm 99$	0.22	$21\pm 8$		_	_	
	c-DOTAP	0.7	6	$112 \pm 41$	0.13	$-12\pm1$		$44\pm2$	1	nd
	c-DOTAP	30	6	$208 \pm 85$	0.16	$10\pm1$	$7 \times 10^{10}$	$40 \pm 3$	6	22
	c-DOTAP	30	6	$215\pm85$	0.16	$24\pm7$		$48\pm2$	60	1
	c-DOTAP	30	6	$209\pm12$	0.34	$26 \pm 5$	$8 \times 10^{10}$	$47\pm1$	230	1
	c-DOTMA	30	4	$163 \pm 61$	0.14	$39 \pm 8$		_	_	_
	c-DOTMA	30	6	$187 \pm 91$	0.21	$38 \pm 6$	$7 \times 10^{10}$	_	_	_
	c-DOTMA	30	8	$172 \pm 99$	0.36	$44 \pm 6$		_	_	_
	c-DOTMA	0.7	6	$150 \pm 53$	0.16	$18 \pm 6$	$2\times10^{11}$	$38\pm2$	6	80
	c-DOTMA	10	6	$169 \pm 77$	0.21	$20\pm1$		$89\pm1$	60	1
	c-DOTMA	30	6	$198 \pm 88$	0.16	$27\pm7$		$90\pm2$	80	1
	c-DOTMA	30	6	$178\pm78$	0.19	$48\pm7$	$3\times10^{11}$	$95\pm1$	250	3

the target site of action. (Yan et al., 2024).

mRNA carriers should ideally have a size range of 50 to 200 nm (Ji et al., 2023). Traditional methods for LNPs manufacturing typically involve creating a lipid layer that is then hydrated with an aqueous buffer containing nucleic acids, allowing for the passive encapsulation of the payload (Roces et al., 2020). However, this approach often forms multilamellar, large, and heterogeneous particles (>100 nm) with low encapsulation efficiency. To achieve the desired particle size, additional post-processing steps such as extrusion or sonication are required (Yu et al., 2009). Furthermore, this method faces challenges in scalability and suffers from poor batch-to-batch reproducibility. The advent of ethanol injection technology, combined with microfluidic techniques or other mixing protocols (Santo et al., 2015, 2014) in the early 2000 s, revolutionized LNP manufacturing. This innovation enabled the production of more efficient and targeted drug delivery systems, improving therapeutic outcomes and scalability (Jahn et al., 2004).

Among different technologies, microfluidics technology has gained widespread recognition in basic research due to its ability to mix fluids under laminar flow and precisely control process parameters, including total flow rate and flow rate ratio, which ensure high batch-to-batch reproducibility and uniformity. These properties make it a valuable platform for developing advanced drug delivery systems, particularly LNPs (Gimondi et al., 2023). However, while its advantages are wellestablished at the bench scale, its scale-up to industrial manufacturing presents significant challenges. On one side, microfluidics offers unique opportunities for industrial-scale applications, as its precision minimizes material waste, a critical factor when working with expensive components like ionizable lipids and nucleic acids. On the other hand, transitioning from bench-scale research to industrial-scale manufacturing involves overcoming several obstacles. Scalability remains a significant challenge, as microfluidic systems are inherently designed for small volumes. Developing more extensive or parallelized microfluidic setups is necessary to meet industrial demands (Wong et al., 2024). Leveraging microfluidics can help manufacturers achieve high production speeds, reduce overall manufacturing time, and maintain consistent quality and performance, which have to comply with regulatory requirements like Good Manufacturing Practices (GMP) (Mehta et al., 2023).

Although the microfluidic technique involves precisely integrating lipids with an aqueous phase containing nucleic acids, process parameters optimization is always required (Ciaglia et al., 2019; Giudice et al.,

2024; Lamparelli et al., 2024). The present work will focus on formulation assembled with cationic lipids, such as DOTAP and DOTMA, which will be used to deliver mRNA encoding Enhanced Green Fluorescent Protein (eGFP). In more detail, a comparative analysis of DOTAP vs. DOTMA formulations will be performed, focusing on their cytotoxicity. A commercially available formulation, Lipid-FLEX (Precigenome, CA, USA), will be used alongside DOTAP and DOTMA for comparison purposes. Microfluidic process parameters, including Total Lipid Concentration and Total Flow Rate (TFR), will be explored to fine-tune particle size distribution (PSD), polydispersity index (PDI), and surface charge (ζ-potential). Single unilamellar vesicle structure will also be the primary goal. The nitrogen-to-phosphate (N/P) ratio, which balances cationic lipid and mRNA, will be adjusted to optimize encapsulation and transfection efficiency. The formulations will be tested on immortalized cell lines (CHO-K1, RAW 264.7, and monocytic THP-1) and primary human peripheral blood mononuclear cells (hPBMCs) to evaluate their toxicity versus effectiveness in eGFP transfection.

### 2. Materials and methods

### 2.1. Lipid nanoparticles formulations (LNPs)

LNPs were produced by microfluidic technology (MF) using the NanoGenerator Flex M (Precigenome LLC San Jose, CA- USA), equipped with a passive microchip. The ethanol phase was prepared using cationic lipid as 1,2-di-O-octadecenyl-3-trimethylammonium propane chloride salt (DOTMA) or 1,2-dioleoyl-3-trimethylammonium-propane chloride salt (DOTAP), with 1,2-distearoyl-sn-glycero-3-phosphocholine (DSPC), cholesterol ovine (Chol) and 1,2-distearoyl-sn-glycero-3-phosphoethanolamine-N-[methoxy(polyethylene glycol)-2000] (PEG2000PE). Commercially available lipid mix composition ( $Lipidflex^{TM}$ ) was also assembled with DOTMA or DOTAP, as indicated by the suppliers (Precigenome LLC, San Jose, CA, USA). All lipids were purchased from AvantiPolarLipids Inc. (Alabaster, Alabama, USA).

mRNA-eGFP, purchased from RIBOPRO (RIB-00624), was tested at concentrations ranging from 6.66 to 26.6  $\mu$ g/mL in buffer sodium acetate 100 mM at pH 5.5. Subsequently, the dialysis step was performed by adopting Slide-A-Lyzer dialysis cassettes with a membrane cutoff of 10 kDa in PBS buffer at pH 7.4. The microfluidic platform was validated as reported elsewhere (Lamparelli et al., 2024).

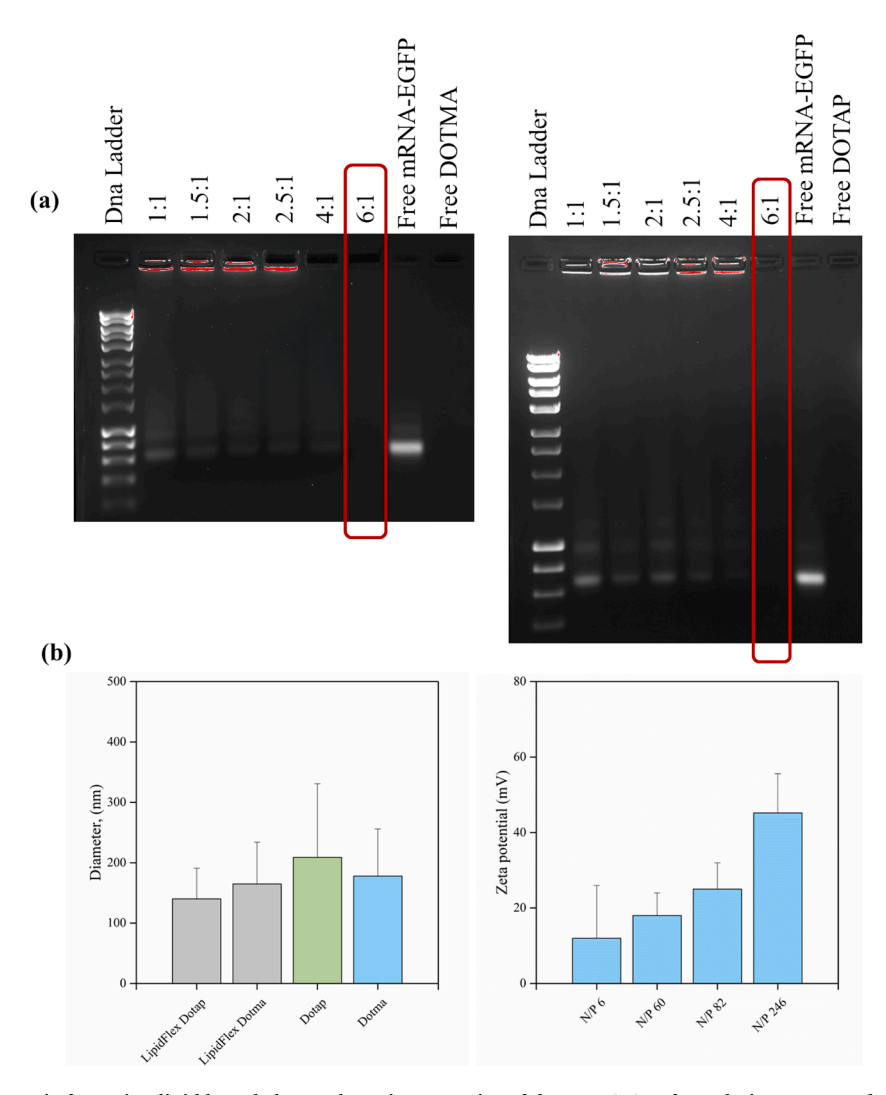


Fig. 4. Evaluation of the N/P ratio for cation lipid by gel electrophoresis, mean size of the mRNA-GFP formulations prepared, and N/P ratio effect on LNPs surface charge. Optimum N/P ratio for both cationic lipids was determined to be 6, as demonstrated in the gel images (a). Mean diameters of all mRNA-GFP formulations at N/P6 ratio (3:1 FRR; 6 mL/min) (b, left side). Surface charge at increasing N/P ratios, attributed to a progressively reduced mRNA payload (b, right side).

### 2.2. N/P ratio by agarose gel retardation assay

The interaction between fixed cationic lipids (DOTMA and DOTAP) and eGFP mRNA was investigated using Gel Retardation Assay (Aydin et al., 2022), adopting the molar ratio between the positively charged groups ("N") and the negatively charged phosphate groups ("P"), named N/P ratio. Precisely, "N" is calculated by multiplying the moles of the cationic lipid by the number of positively charged groups in its structure. In contrast, "P" corresponds to the mRNA moles multiplying the number of negatively charged phosphate groups. This ratio describes the charge balance and complexation efficiency between the lipid and the mRNA, as indicated in eq. (1).

$$\frac{N}{p} \text{ ratio } = \frac{\text{moles of cationic lipid} \times \text{positive groups per molecule}}{\text{moles of mRNA} \times \text{number of nucleotides}}$$
(1)

Cationic lipids (1 mg/mL) were added at different N/P ratios (1:1, 1.5:1, 2:1, 2.5:1, 4:1, 6:1) to 1  $\mu$ g of mRNA-eGFP in RNAse-free water. All mixes were incubated at room temperature for 30 min. Then, Loading Dye containing 30 % (v/v) glycerol, 0.25 % (w/v) bromophenol blue, and 0.25 % (w/v) xylene cyanol FF (6X) was added and samples loaded on 1 % agarose gel with GelRed® Nucleic Acid Gel Stain 1X (Biotium, Fremont, CA). Electrophoresis was performed at 60 V for 2 h in 1x TAE

running buffer (pH 8.0). The bands were monitored by UV using a ChemiDoc XRS+ (BioRad).

### 2.3. Lipid nanoparticles size, distribution, $\zeta$ -potential and concentration

The dynamic light scattering (DLS) technique, using ZetaSizer (model 1000HSa, Malvern, UK) at 25 °C, equipped with a 633 nm He-Ne laser and a 173C detector angle, was employed to measure particle sizes, distributions, and  $\zeta$ -potential. NanoSight NS300 (Malvern Panalytical, Westborough, MA) was adopted to evaluate LNP concentrations. All measurements were conducted in triplicate for each sample just after production and after 60 days, following storage at 4 °C to ascertain product stability.

## 2.4. Lipid nanoparticles morphology and structure by SEM and TEM imaging

Vesicle morphology was analyzed using field emission-scanning electron microscopy (FE-SEM, model LEO 1525, Carl Zeiss SMT AG, Oberkochen, Germany). Multiple droplets were deposited onto a double-sided adhesive carbon tape attached to an aluminum stub and dried with a critical point dryer (model K850, Quorum Technologies Ltd, East Sussex, United Kingdom). The samples were then coated with a thin gold

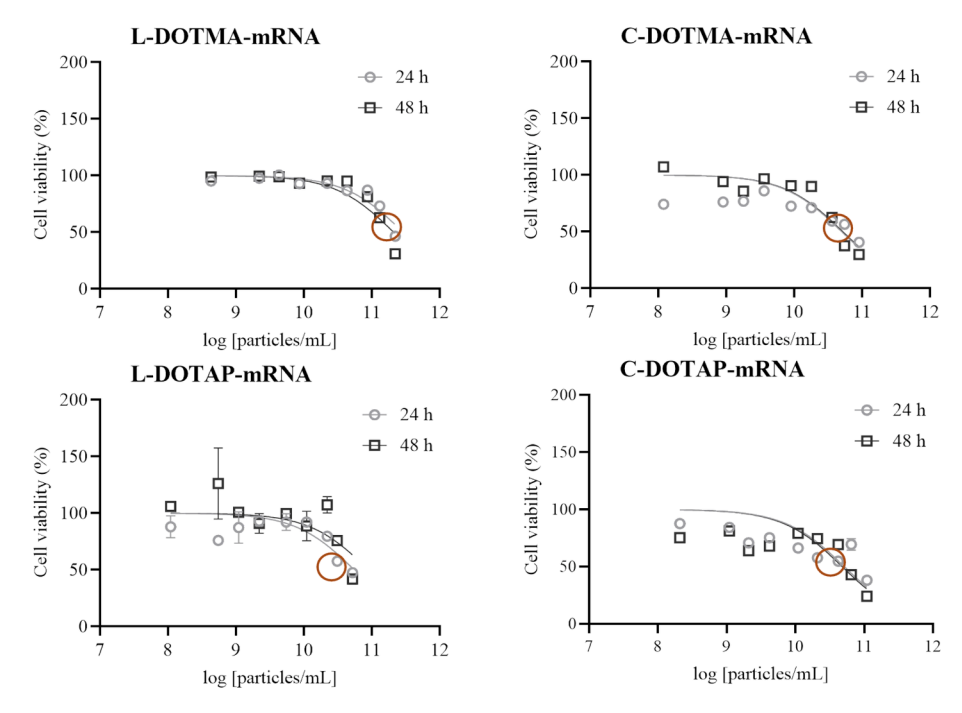


Fig. 5. Cell viability data and IC<sub>50</sub> values of empty and mRNA-loaded formulations (N/P250) measured in CHO-K1 cell line. The collected data indicated an IC<sub>50</sub> value on the order of  $10^{11}$  LNPs/mL for the c-DOTMA-mRNA formulation after 24 h, slightly lower to that of the commercial *LipidFlex*-DOTMA-mRNA formulation. Similarly, the c-DOTAP-mRNA formulation displayed an IC<sub>50</sub> value of  $8 \cdot 10^{10}$  closely matching the *LipidFlex* formulation with the same cationic lipid. N/P 250 was chosen to minimize mRNA contribution in the present evaluation and mainly focusing on formulation toxicity.

layer (approximately 250 Å thick) using a sputter coater (model 108 A, Agar Scientific, Stansted, United Kingdom).

LNP morphology was also observed using a Transmission Electron Microscope (TEM). To capture TEM micrographs, 8  $\mu l$  of each diluted sample were dropped on a Formvar/Carbon 200-mesh Cu Agar Scientific Ltd. (Ted Pella, USA Cat. No. 01800-F). Negative staining was then performed using a phosphotungstic acid solution (2 % w/v) directly made on the deposit for 60 s. The samples were finally air-dried overnight. The resulting images were obtained using bright-field mode (TEM mod. FEI TECNAI G2 200 kV S-TWIN equipped with a 4 K camera; electron source with LaB6 emitter; FEI Inc., Dawson Creek Drive, Hillsboro, OR, USA). Images were taken at 120 kV using a spot size of 3 and an integration time of 1 s.

### 2.5. mRNA encapsulation efficiency

Encapsulation Efficiency of mRNA-eGFP was performed using the RediPlate  $^{\rm TM}$  96 RiboGreen  $^{\rm TM}$  RNA Quantitation Kit (Thermo Fisher Scientific). The calibration curve was set from 0 to 1000 ng/mL. RNA standards and experimental samples (PBS after dialysis) were added to the assay wells and incubated for 20 min at Room Temperature, protected from light. Fluorescence was measured using a fluorescence-based microplate reader (Infinite 200 PRO, Tecan) with excitation light and filter settings for standard fluorescein wavelengths (excitation  $\sim$  480 nm, emission  $\sim$  520 nm). Encapsulation Efficiency was calculated using the direct analytical method using 1 uL of the LNs with TRITON 0.2 %.

### 2.6. Cytotoxicity assay by MTT in Ovarian Hamster cell line (CHO)

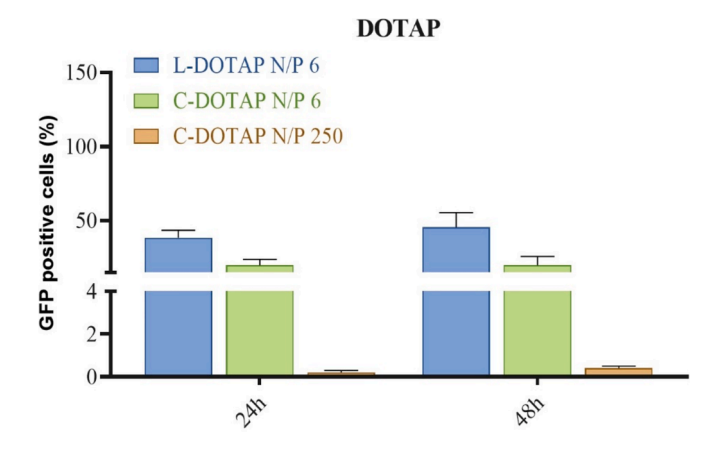
Chinese Hamster Ovary Cells sub-clone K1 (CHO-K1, ATCC® CCL- $61^{TM}$ ) were seeded in 96-well plates at a density of 10.000 cells/well and cultured in DMEM-F12 medium (Aurogene, Rome, Italy) supplemented with 10 % FBS (Gibco) and 1 % penicillin/streptomycin (50 U/mL) (Corning Cellgro, Manassas, VA, USA) and incubated in a humidified atmosphere containing 5 % CO<sub>2</sub> and 95 % air. Empty and mRNA-eGFP

loaded LNPs were tested at the following concentrations: 1, 5, 10, 20, 50, 100, 200, 300, and 500  $\mu$ g/mL, which correspond to a number ranging from  $10^9$  up to  $10^{11}$  LNPs/mL. They were incubated for 24 h and 48 h at 37 °C and 5 % CO<sub>2</sub>. Cell metabolic activity was monitored by 3-(4,5-Dimethylthiazol-2-yl9-2,5-diphenyl-tetrazolium bromide (MTT) assay used at a final concentration of 0.5 mg/mL. Following the incubation period, 20  $\mu$ L of MTT was added to the culture media and incubated for 4 h. Subsequently, formazan crystals were dissolved in 200  $\mu$ L of dimethyl sulfoxide (DMSO). Absorbance was measured at 490 nm using a microplate reader (Infinite F200 PRO, Tecan Group Ltd., SW). The experiments were performed in triplicate (n = 3). Cell metabolic activity was calculated as a percentage compared to the control group (considered as 100 %), according to equation (2).

$$\mbox{Cell metabolic activity (\%)} \ = \ \frac{|\mbox{of}|\mbox{sample} - |\mbox{of}|\mbox{blank}}{|\mbox{of}|\mbox{control} - |\mbox{of}|\mbox{blank}} \ x \, 100 \eqno(2)$$

# 2.7. mRNA-eGFP expression by confocal microscope in Ovarian Hamster cell line (CHO-K1)

CHO-K1 cells were seeded at  $1 \times 10^6$  cells/mL in 12-multiwell plates on 13 mm Microscope Glass Slides and treated with different concentrations of empty and mRNA-eGFP loaded LNPs from  $10^9\ \text{up}$  to  $10^{11}$ LNP/mL. The adoption of LNP concentrations expressed as a number per mL was chosen as this value was experimentally checked with Nanoparticle Tracking Analysis (NTA), whereas the value of mg/mL was calculated from fabrication process dilution. This approach ensures a stronger consistency across the comparison of different formulations. After 24 h and 48 h of incubation, CHO-K1 cells were fixed in 2 % paraformaldehyde (PFA, Sigma) for 30 min at RT. Subsequently, cells were washed with PBS 1X and counterstained using 4',6-diamidino-2phenylindole (DAPI). All images were acquired at 63x magnification with identical settings of light, exposure time, and gain using a Leica laser-scanning confocal microscope (mod. TCS SP5; Leica Microsystems, Wetzlar DE). Alternatively, after incubation, CHO-K1 cells were detached and resuspended in PBS 1X for acquisition.



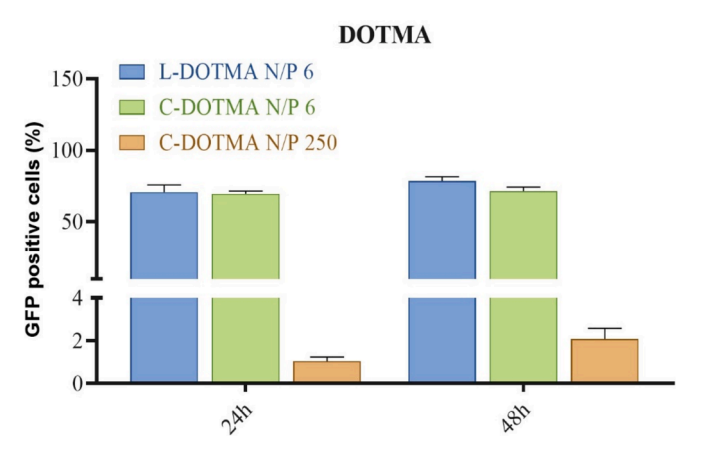


Fig. 6. eGFP transfection efficiency on CHO-K1 cell line by flow cytometry. CHO-K1 cells were cultured with c-DOTMA and c-DOTAP mRNA-eGFP formulations (N/P 250 and N/P 6), with a fixed concentration of  $2\times 10^{10}$  LNPs/mL (i.e.; below IC $_{50}$  values), for 24 and 48 h. The commercial *Lipidflex* formulations were also tested for comparison. Results confirmed GFP expression at 24 and 48 h, with higher efficiency observed for the c-DOTMA formulation. Notably, the N/P ratio 6 outperformed the N/P ratio 250.

# 2.8. Cytotoxicity assay by flow cytometry in human PBMCs and THP-1 cells

Propidium Iodide (PI) staining was used to assay the cytotoxicity of mRNAeGFP loaded DOTMA and DOTAP formulations at concentrations ranging from  $10^9$  up to  $10^{11}$  LNP/mL for 6 h, 24 h, and 48 h on PBMCs, THP-1 and RAW264.7 cells. After treatment, 800.000 cells were resuspended in Hank's Balanced Salt Solution (HBBS, Gibco), centrifuged, and stained with PI (1µg/mL; Miltenyi Biotec, Bergisch Gladbach, Germany). After 15 min incubation in the dark, FACS analysis was performed. For each test, cells were analyzed using a FACSVerse flow cytometer (BD Biosciences, Swindon, UK).

### 2.9. mRNA-eGFP expression in human primary PBMCs and human THP-1 cells

Human Peripheral Blood Mononuclear Cells (PBMCs) were extracted from whole blood by density gradient (Ficoll). After separation, PBMCs were collected and washed for the subsequent experiments. PBMCs and THP-1 were seeded at  $3\times10^6$  cells/mL in 12-multiwell plates in RPMI-1640 medium (Gibco®, Thermo Fisher Scientific, Waltham, MA, USA) supplemented with 10% (v/v) fetal serum bovine (FBS, Gibco®, Thermo Fisher Scientific, Waltham, MA, USA), 1% (v/v) penicillin–streptomycin (Aurogene, Rome, Italy), 1% (v/v) MEM non-essential amino acids

(MEM NEAA, Gibco®, Thermo Fisher Scientific, Waltham, MA, USA), and 1 % (v/v) sodium pyruvate (Aurogene, Rome, Italy) and incubated in a humidified atmosphere containing 5 % CO2 and 95 % air for the subsequent experiments. PBMCs and/or THP-1 cells were treated with different concentrations of mRNA-eGFP loaded DOTMA and DOTAP LNPs ranging from 10<sup>9</sup> to 10<sup>11</sup> LNP/mL for 6 h, 24 h, and 48 h. After incubation, PBMCs and THP-1 were detached for FACS acquisition. Besides the GFP and to characterize the different PBMC populations, PBMCs were stained even with mAb against human CD19-PE (Miltenyi Biotec, Bergisch Gladbach, Germany), CD3-PEVio (Miltenyi Biotec, Bergisch Gladbach, Germany), CD14 PerCP Cy5.5 (BioLegend, San Diego, CA, USA), CD11b APC (BioLegend, San Diego, CA, USA). After 30 min incubation at 4 °C in the dark, cells were washed, centrifuged, and resuspended in staining buffer for the FACS analysis. For each test, cells were analyzed using a FACSVerse flow cytometer (BD Biosciences, Swindon, UK).

### 2.10. mRNA-eGFP expression in murine RAW264.7 (macrophage-like)

RAW264.7 (macrophage-like, Abelson leukemia virus-transformed cell line derived from BALB/c mice) were seeded at 200.000 cells/mL in 12-multiwell plates in DMEM medium (Gibco®, Thermo Fisher Scientific, Waltham, MA, USA) supplemented with 10 % (v/v) fetal serum bovine (FBS, Gibco®, Thermo Fisher Scientific, Waltham, MA, USA), 1 % (v/v) penicillin–streptomycin (Aurogene, Rome, Italy), 1 % (v/v) MEM non-essential amino acids (MEM NEAA, Gibco®, Thermo Fisher Scientific, Waltham, MA, USA), and 1 % (v/v) sodium pyruvate (Aurogene, Rome, Italy) and incubated in a humidified atmosphere containing 5 % CO2 and 95 % air for the subsequent experiments. RAW264.7 were treated with different concentrations of mRNA-eGFP loaded DOTMA and DOTAP LNPs at concentrations varied from 109 up to 1011 LNP/mL for 6 h, 24 h, and 72 h. After incubation, RAW264.7 cells were detached for FACS acquisition of GFP positivity.

### 3. Results & discussion

### 3.1. Optimization of formulation and microfluidic parameters

A schematic representation of the microfluidic chip adopted is reported in Fig. 1a. The illustration showcases a streamlined microfluidic setup for the ethanol injection method in LNP synthesis. Key components include the inlet channels; one carries a lipid solution dissolved in ethanol, while the other delivers an aqueous sodium acetate buffer (pH 5.5, 100 mM) containing, eventually, nucleic acids (e.g., mRNA). An acidic buffer was employed despite DOTAP and DOTMA being cationic lipids without pH-dependent charge conversion; the choice was related to several reasons, such as consistency with established protocols, stability of LNP formation, and impact on Encapsulation Efficiency. Indeed, acidic buffers are standard practice in preparing LNPs, ensuring comparability with other studies and protocols. This choice allows for easier benchmarking of the results (Leung et al., 2014). Furthermore, even in the absence of ionizable lipids, an acidic environment can enhance the stability of the nanoparticle assembly process, potentially influencing the encapsulation efficiency of mRNA and the uniformity of the particles (Larson et al., 2022). Finally, acidic buffers can promote the interaction between the negatively charged mRNA and the cationic lipids during particle formation, optimizing encapsulation (Schober et al., 2024).

The microfluidic mixing circuit selected is a passive staggered herringbone micromixer (SHM) with a Y-geometry fabricated in Topas® COC, featuring the following dimensions: an inlet channel width of 300  $\mu m$ , a mixer and outlet channel width of 600  $\mu m$ , a channel depth of 200  $\mu m$ , and a total length of 20 mm. Fluid streams converge at controlled flow rates, facilitating rapid mixing and driving the spontaneous self-assembly of LNPs. Total Flow Rate (TFR) and Flow Rate Ratio (FRR) were explored because they regulate the mixing dynamics, influencing

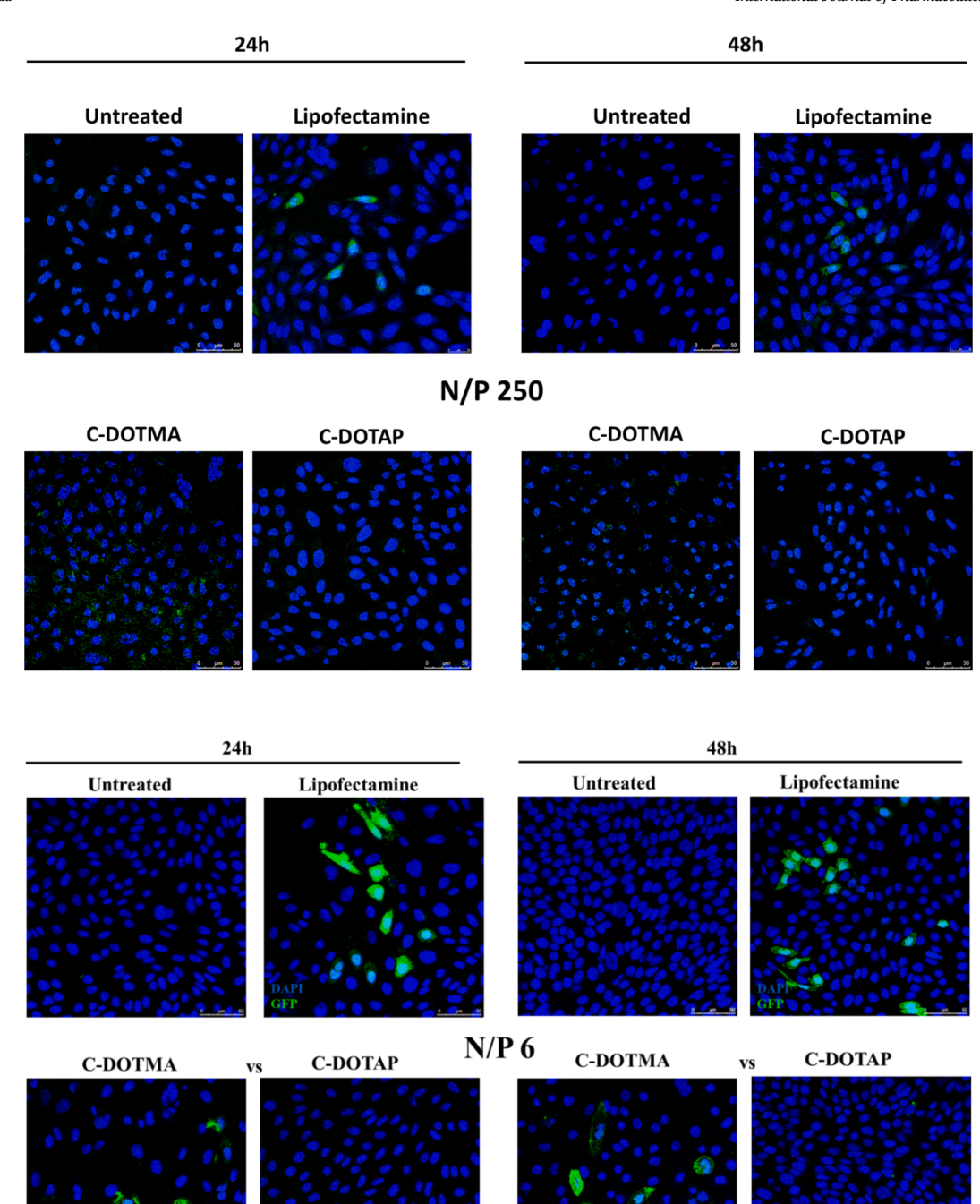
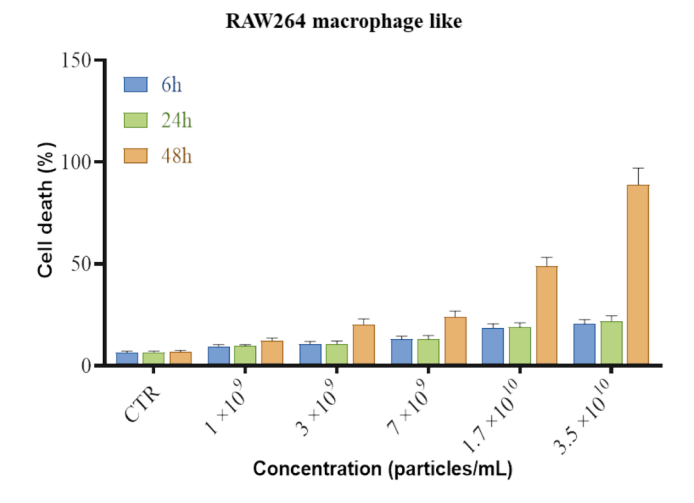


Fig. 7. eGFP transfection efficiency observed in CHO-K1 cell line by confocal microscopy. CHO-K1 supplemented with c-DOTMA and c-DOTAP mRNA-eGFP formulations (N/P 6 and N/P 250) at fixed concentration of  $2 \times 10^{10}$  particles/mL (which is lower than IC<sub>50</sub> values) for 24 h and 48 h. Untreated CHO-K1 were negative control; transfection with Lipofectamine was used as a positive control. All confocal images were captured at 63x magnification. At N/P ratio of 6 for c-DOTMA formulation confirmed a better eGFP-mRNA transfection. Scale bar: 50  $\mu$ m.

### LNP size and homogeneity.

DOTMA and DOTAP cationic lipids were selected for performance evaluation in all formulations investigated. Known for their ability to interact with negatively charged nucleic acids, those two cationic lipids are crucial in facilitating nucleic acid encapsulation and delivery. Structurally, DOTMA features two ether bonds, while DOTAP contains two ester bonds. Despite this difference, both lipids have effectively bound mRNA (Sun and Lu, 2023). In this study, these lipids were formulated using a commercial *LipidFlex*® mix (of unspecified

composition), as per provided instructions, and a customized lipid mixture was developed and evaluated here. The custom formulation (c-) included DSPC, cholesterol, and PEG-2000 PE prepared in ethanol with a molar ratio of 10:38.5:1.5 plus 50 of cationic lipid. The molar ratios for DSPC, cholesterol, and PEG-2000 PE (10:38.5:1.5), along with 50 % cationic lipid, were selected based on a combination of established literature and empirical optimization. This specific ratio was designed to achieve an optimal balance between structural stability, membrane fusion potential, and steric hindrance that are key factors for efficient



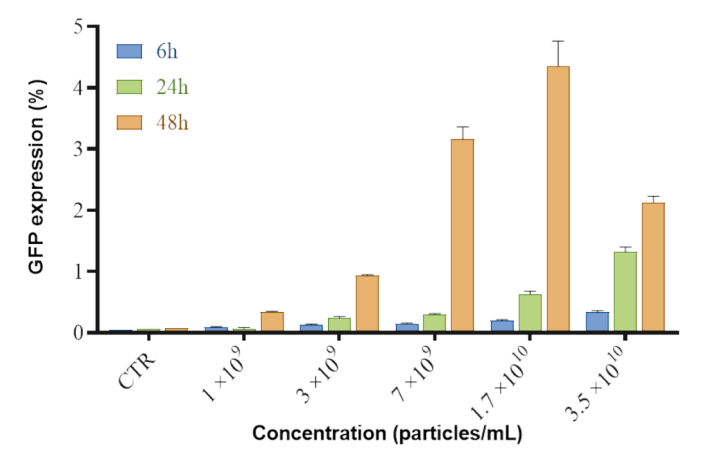


Fig. 8. Cytotoxicity and eGFP transfection efficiency in RAW264-macrophage like measured by flow cytometry Data acquired supplementing c-DOTMA (N/P250) at different concentration (between  $10^8$  and  $10^{10}$  LNP/mL) on RAW murine macrophage-like line. High toxicity was observed for concentration higher than  $1\times 10^{10}$  LNP/mL. eGFP expression of 3.5 % was observed at  $7\times 10^9$  LNPs/mL after 48 h.

mRNA encapsulation and delivery. DSPC contributes to a rigid bilayer structure, cholesterol enhances membrane fluidity and overall stability, while PEG-2000 PE minimizes non-specific interactions and prolongs nanoparticle circulation time in vivo. The 50 % cationic lipid content was fine-tuned to ensure strong electrostatic interactions with the negatively charged mRNA, resulting in high encapsulation efficiency while maintaining particle stability and minimizing cytotoxicity.

For the initial trials, the total lipid concentration in the ethanol solution was set at 30 mM, consistent with the commercial LipidFlex formulation, and this value was not exceeded. Using this fixed concentration, various total flow rates (TFR) ranging from 4 to 8 mL/min were tested while maintaining a flow rate ratio (FRR) of 3:1. As the TFR increased from 4 to 8 mL/min, an increase in the mean size of LNPs was observed for c-DOTAP formulations, ranging from  $189\pm75$  nm to  $223\pm99$  nm. In contrast, c-DOTMA formulations showed less consistent size variation, with mean sizes ranging from  $163\pm61$  nm to  $187\pm91$  nm; a slightly larger distribution was observed at lower flow rates. Starting from a TFR of 6 mL/min, the pressure curve within the microfluidic channel demonstrated the highest stability throughout the production process (see Fig. 1b). Consequently, this flow rate was selected as the optimal TFR for further formulations.

With the TFR fixed at 6 mL/min, the Flow Rate Ratio (FRR) was varied between 3:1 and 2:1. When an FRR of 2:1 was tested, an extremely low mass recovery was observed (data not shown), and this

ratio was excluded from further exploration. The lipid concentration was adjusted to 1, 10, and 30 mM significantly influencing the LNPs' mean size and distribution. A decrease in mean size was observed, as lipid concentration decreased from 30 to 1 mM for both customized formulations (see distribution curves in Fig. 2b). PDI index also shrunk from 0.2 to 0.13, approaching the monodisperse value. As SEM micrographs showed, both customized formulations (C-DOTAP and C-DOTMA) exhibited a spherical shape with highly uniform morphology. The partial vesicle agglomeration observed in SEM was primarily attributed to the drying process during sample preparation. TEM imaging further confirmed the presence of a Single Unilamellar Vesicle (SUV) structure (see Fig. 3). These findings reflect the efficiency of the proposed process and emphasize the robustness of the optimized process parameters. All data mentioned are also summarized in Table 1.

### 3.2. mRNA-eGFP N/P ratio optimization and LNP surface charge

To evaluate the affinity between eGFP-mRNA and cationic phospholipids (DOTMA or DOTAP), a gel retardation assay was conducted. Cationic phospholipids and eGFP-mRNA were prepared in different nitrogen/phosphate (N/P) ratios and loaded onto the gel. The N/P ratio refers to the ratio of nitrogen (N) from ammine in cationic lipids to phosphorous (P) from phosphate groups from mRNA, which is a key parameter in determining the efficiency of mRNA encapsulation.

Our findings, depicted in Fig. 4a, demonstrated the successful binding between the nucleic acid and cationic phospholipids, as documented by the lack of the eGFP mRNA band in the gel. Notably, mRNA binding for both cationic phospholipids was observed at an N/P ratio value of 6, indicating the complete complexation between the mRNA and cationic phospholipids in both cases at the same N/P ratio value. These findings are consistent with previous studies and confirm the effective interaction between the mRNA and cationic phospholipids.

mRNA-eGFP formulation was obtained operating at an optimized FRR of 3:1 with TFR of 6 mL/min by adding the nucleic acid in the aqueous phase (sodium acetate pH 5.5 100 mM). In the case of c-DOTAP and c-DOTMA formulations, mRNA-eGFP was loaded at various N/P ratios ranging from 6 to 250 by the need to investigate the effects of nucleic acid (N, negatively charged) to lipid (P, positively charged) ratios on the physicochemical properties of LNPs. To increase the N/P ratio of formulations, the mRNA loaded in water phase was always fixed at 6.66 ug/mL and lipid fraction in oily phase was progressively reduced (see more details Table 1). The range of 250 to 6 ensures coverage of lipid-rich and nucleic acid-rich formulations, helping to identify trends across a broad spectrum and ensuring no critical regions of the formulation space are overlooked. Significant physicochemical changes often occur at specific thresholds, such as optimal charge ratios for nucleic acid encapsulation or LNP stability. This range allows for the observation of those transitions and the identification of the transition point (Chen et al., 2024). Indeed, higher N/P ratios may favor improved encapsulation efficiency (EE, %) because of an excess of positively charged lipids available to bind nucleic acids; both extremes of the N/P ratio can lead to changes in size, polydispersity and stability, while nucleic acid excess (low N/P) might reduce zeta potential or destabilize LNPs (McKenzie et al., 2023).

A linear increase in positive surface charge was observed as the ratio values increased at increased N/P ratio due to a progressively reduced mRNA payload (see Fig. 4b). This observation is consistent with the literature and testifies to the accuracy and high reproducibility of the formulation parameters chosen. This ratio directly influences the surface charge ( $\zeta$ -potential) of the LNPs; at lower N/P ratio values, because all cationic charges are saturated by the loaded mRNA, the vesicles typically may have an almost neutral surface charge, as there is no excess of amine groups; in our cases,  $\zeta$ -potential values of 18 mV were measured with an N/P ratio of 6. Increasing the N/P values, the vesicle's surface charge becomes more positive, showing a higher  $\zeta$ -potential up to 48 mV due to the excess amine groups not involved in balancing the mRNA's

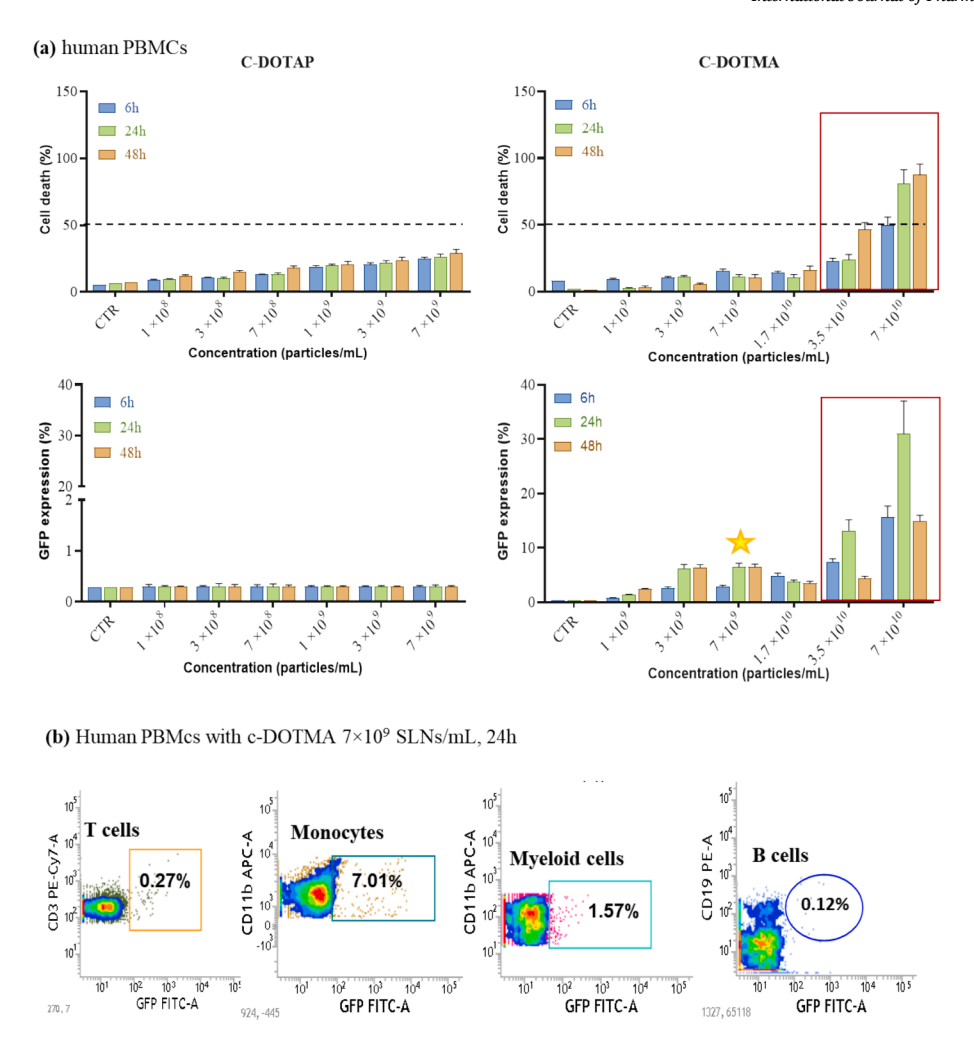


Fig. 9. (a-c). Cytotoxicity data and eGFP transfection efficiency in human PBMC population measured by flow cytometry. Data acquired supplementing c-DOTAP and c-DOTMA formulations (N/P250) at increasing concentrations (between  $10^8$  and  $10^{10}$  LNP/mL) for 6, 24, and 48 h; c-DOTMA formulation seemed extremely good in eGFP transfection even if toxicity was revealed at concentration equal or higher than  $3.5 \times 10^{10}$  LNP/mL. At concentration of  $7 \times 10^9$  LNP/mL was observed 7.5 % of GFP expression, with acceptable toxicity (a). Representative dot blot of flow cytometry analysis of eGFP expression percentage in immune cells among hPBMCs after treatment with c-DOTMA at a concentration of  $7 \times 10^9$  LNPs/mL for 24 h (b).

negative charge. This trend was further confirmed with c-DOTAP formulation; furthermore, when the N/P ratio was set at 1 (below the optimal value of 6), an LNPs negative surface of  $-12\,\mathrm{mV}$  was measured. As the N/P ratio increased to 250, the excess of positive charge from the cationic lipids significantly enhanced the encapsulation of negatively charged mRNA, achieving the highest encapsulation efficiency, close to 90 %, as observed for example for c-DOTMA formulation. In contrast, same formulation at N/P ratio of 6 showed an encapsulation efficiency of approximately 38 %. The c-DOTAP formulation consistently demonstrated always lower encapsulation efficiencies, at around 40–45 %, regardless of the N/P ratio. From this data, it is clear that the adjustment of formulation N/P ratio plays a crucial role in optimizing both the mRNA loading and the surface characteristics of the system, which can affect not only its stability but further cellular uptake and transfection efficiency.

### 3.3. Cytotoxicity ( $IC_{50}$ ) and transfection in CHO-K1 cell line

The half-maximal inhibitory concentration (IC $_{50}$ ), representing the concentration required to reduce cell viability or inhibit growth by 50 %, was determined at 24 and 48 h using the MTT assay on CHO-K1 cells (see Table 1 and Fig. 5). Formulations with the lowest amount of mRNA (i.e.; N/P250) were selected for cytotoxicity study in order to exclude a relative toxicity of mRNA loaded. With this assumption we may

reasonable attribute the observed toxicity, only at the lipid composition of the LNPs. For the LF-DOTMA-eGFP-mRNA formulation (N/P ratio 240), the IC $_{50}$  value was  $8\cdot 10^{10}$  LNP/mL, at 24 h. In contrast, the customized DOTMA formulation (c-DOTMA) with the almost similar N/P ratio exhibited significantly higher value of  $3\cdot 10^{11}$  LNP/mL, indicating lower cytotoxicity for the customized formulation. For the LF-DOTAP-eGFP-mRNA formulation (N/P ratio 230), the IC $_{50}$  was  $8.6\cdot 10^{10}$  LNP/mL at 24 h. The customized DOTAP formulation (c-DOTAP) with the same N/P ratio showed similar IC $_{50}$  of  $8.8\cdot 10^{10}$  LNP/mL. This suggests similar cytotoxicity behavior between the commercial and customized formulations in the case of DOTAP. The data highlight that while the DOTAP-based formulations demonstrate comparable cytotoxicity across customized and commercial formulations, the DOTMA-based custom formulation shows markedly lower cytotoxicity than its commercial counterpart.

Transfection efficiency was evaluated by flow cytometry on CHO-K1 cells for all formulations at both N/P ratios of 250 and 6, after 24 and 48 h (Fig. 6). A concentration of  $2\times 10^{10}$  LNP/mL (well below IC $_{50}$  values) was used. For formulations with an N/P ratio of 6, the LF-DOTAP formulation outperformed the customized c-DOTAP, achieving a transfection efficiency of approximately 40 % after 24 h, compared to 20 % for c-DOTAP. However, at an N/P ratio of 250, both DOTAP formulations showed low transfection efficiency, with a maximum of 1 % for the customized version. In contrast, the c-DOTMA formulation exhibited

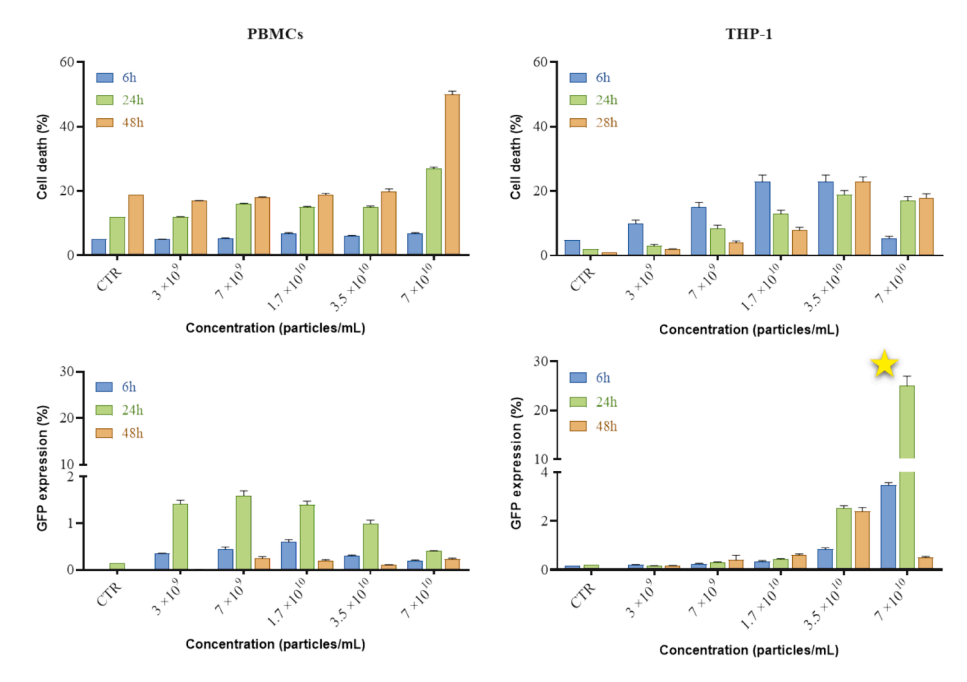


Fig. 10. Cytotoxicity and eGFP transfection efficiency in human PBMC population and THP-1 cell line measured by flow cytometry. Data acquired supplementing c-DOTMA mRNA-eGFP formulation (N/P6) at increasing concentrations (between  $10^8$  and  $10^{10}$  LNP/mL) for 6, 24, and 48 h. The cytotoxicity and percentage of eGFP expression are shown, indicating formulation good performance, especially with THP-1 at concentration of  $7 \times 10^{10}$  LNP/mL where 25 % of expression was monitored.

transfection efficiency similar to that of LF-DOTMA, of about 80 % and 70 %, respectively, after 24 h, at an N/P ratio of 6. At an N/P ratio of 250, the c-DOTMA formulation showed modest transfection efficiencies of 1 % and 3 % after 24 and 48 h, respectively. These results indicate that formulations based on DOTAP consistently demonstrated lower transfection efficiency compared to DOTMA-based formulations, highlighting the superior performance of DOTMA as a carrier for mRNA delivery. Insufficient transfection efficiency of c-DOTAP is likely influenced by multiple factors, including lipid structure, surface charge, particle size, and mRNA encapsulation efficiency. Furthermore, DOTAP's rigid structure due to saturated lipid tails can lead to less flexible lipid nanoparticles, potentially reducing membrane fusion and endosomal escape efficiency (Tang et al., 2023). Indeed, despite c-DOTAP imparts a high positive zeta potential to LNPs, which enhances electrostatic interactions with negatively charged cell membranes, an excessive charge can cause cytotoxicity or destabilize the LNP in biological environments (e.g., leading to serum protein adsorption and rapid clearance). Furthermore, high positive charge may also reduce the efficiency of escape from endosomes, as overly cationic particles can get trapped in electrostatic interactions within the endosomal compartment. All these interaction may cause the poor transfection efficiency observed (Mehta et al., 2024).

Good transfection performance was also observed for LF-DOTMA formulation, that is a commercially available of unknown lipid composition (except for the cationic lipid added). LF-DOTMA was studied in the present work only for comparison purpose. Indeed, because of the unknown composition, LF-DOTMA formulation introduces variability and unpredictability in results mainly due to lack of detailed knowledge of its lipid components, preventing to explain any of the observed effects.

The transfection efficiency of customized formulations at N/P ratio of 250 and 6 were also evaluated by confocal microscopy; in such case lipofectamine was used as a control. Transfection experiments were performed using concentrations of  $2\times10^{10}$  LNP/mL for 24 and 48 h, that is well below and near the IC $_{50}$  threshold, as previously discussed. Images revealed an always poor eGFP expression for N/P 250 formulations and only few cells supplemented with the c-DOTMA showed

some faint gray spots. Slight cellular toxicity can be also observed in few degraded nuclei structure highlighted in blue (see Fig. 7a). In case of N/P ratio 6 ratio, very well transfection was assessed at both 24 and 48 h (Fig. 7b). The results showed robust eGFP expression in the treated samples, indicating effective transfection performance with the c-DOTMA formulation.

### 3.4. Murine macrophage RAW264.7 assay by flow cytometry

Cytotoxicity and eGFP expression of c-DOTMA formulation (N/P 250) was also evaluated in the murine macrophagic RAW264.7 cell line at 6, 24, and 72 h. The experiments utilized a dose–response approach with concentrations ranging from order of magnitude  $10^9$  up to  $10^{10}$  LNP/mL (see Fig. 8). In comparison to the CHO cell line, a similar transfection efficiency of 3.5 % after 48 h was observed with a reduced concentration of  $7\times10^9$  particles/mL ( $\approx\!62.5$  ng/mL eGFP-mRNA), but this was accompanied by increased cytotoxicity of approximately 20 %. These results emphasize the importance of optimizing tailored formulations to strike a balance between maximizing transfection efficiency and minimizing cytotoxic effects, particularly for more delicate immune cells such as macrophages.

### 3.5. Human primary PBMCs and THP-1 assay by flow cytometry

The transfection efficiency of c-DOTAP and c-DOTMA formulations were also systematically analyzed using flow cytometry on human Peripheral Blood Mononuclear Cells (hPBMCs). These primary cells served as a high-throughput model for further exploring formulation cytotoxicity on primary human cells.

For customized formulations (N/P 250), concentrations ranging from  $1\times 10^8$  to  $7\times 10^{10}$  LNP/mL were tested, with data collected at 6, 24, and 48-hour intervals to capture dose–response patterns (see Fig. 9a). Although the concentrations used were well below the IC $_{50}$  determined for the CHO cell line, the c-DOTMA formulation at concentrations exceeding 1  $\times$  10 $^{10}$  LNP/mL triggered significant cytotoxicity, affecting 30–50 % of the cell population after 24 and 48 h (highlighted by the red square in Fig. 9a), despite exhibiting high eGFP

expression of up to 30–35 % at 24 h. Interestingly, at concentrations below  $1\times 10^{10}$  LNP/mL, the c-DOTMA formulation showed reduced cytotoxicity ( $\approx\!15\text{--}20$  %) and achieved a notable transfection efficiency of  $\approx\!6.5$  % within 6 h at  $7\times 10^9$  LNP/mL ( $\approx\!62.5$  ng/mL eGFP-mRNA). This transfection rate significantly exceeds the 1 % efficiency observed in CHO cells, but the difference can be likely attributable to variations in detection timing and to the inherent properties of the two cell types. In contrast, data for the c-DOTAP formulation (N/P ratio of 250) confirmed consistently low cytotoxicity across an even higher concentration range. However, this formulation was ineffective in inducing transfection in human PBMCs, showing no measurable transfection efficiency at any tested concentration (Fig. 9a). These findings confirmed the superior performance of c-DOTMA in terms of functional transfection in hPBMCs, while c-DOTAP's lack of transfection capability highlights its limitations in this context.

The c-DOTMA (N/P 250) behavior in hPBMCs was further investigated to examine its cell-specific uptake tendencies. Differences in immune cell membrane composition and endocytosis mechanisms were considered as potential factors influencing this selectivity. Using extensive multiparametric FACS analysis (Fig. 9b), the expression of eGFP was measured across various immune cell subtypes, including CD3+ T cells, CD14+ monocytes, CD11b+ macrophages, and CD19+ B cells. The analysis revealed that transfection was predominantly restricted to CD14+ monocytes, achieving a transfection efficiency of 7% at a concentration of  $7\times10^9$  LNP/mL ( $\approx\!62.5$  ng/mL eGFP-mRNA). This cell-specific targeting underscores c-DOTMA's ability to preferentially transfect monocytes, suggesting potential applications in immune modulation and therapies targeting monocyte-related pathways.

c-DOTMA with an N/P ratio of 6 demonstrated superior performance compared to N/P 250 in CHO cells, prompting further investigation of this specific formulation in human PBMCs, with a particular focus on CD14 + monocytes. Despite the anticipated improved transfection efficiency of the N/P 6 formulation, eGFP positivity was observed to range between 1.4 % and 1.6 % following treatment with concentrations of 3  $\times$  10<sup>9</sup> or 7  $\times$  10<sup>9</sup> LNPs/mL at 24 h (see Fig. 10). Cytotoxicity, resulting in approximately 15 % cell death, was also reported at the tested concentrations and time points for the N/P 6 ratio, as also shown in Fig. 10. Notably, higher concentrations were associated with increased toxicity. The lower transfection efficiency and higher cytotoxicity observed for c-DOTMA at N/P6 in human PBMCs, compared to the same formulation at N/P250, despite the opposite performance trend in CHO cells, may be attributed to inherent differences in cell types. Specifically, the difficulty in transfecting primary immune cells, suboptimal intracellular trafficking, and concentration-dependent membrane toxicity likely played

To further explore the monocyte-specific uptake behavior of c-DOTMA N/P6, we tested the formulation in the monocytic THP-1 cell line. THP-1 is a human leukemia-derived monocytic cell line widely used as a model to study monocyte/macrophage functions, signaling pathways, and immune modulation. As shown in Fig. 10, the results demonstrated significantly higher eGFP positivity rates (ranging from 2.5 % to 25 %) compared to those observed in the total PBMC population under similar conditions. This reinforces the notion that our customized formulation prefers uptake by monocytes, allowing for their selective transfection, and highlights the potential of this formulation for targeted delivery to monocytic cells.

### 4. Conclusion

The c-DOTMA formulation emerged as the most effective, combining reduced cytotoxicity with high, cell-specific transfection efficiency, particularly targeting CD14 + monocytes. This selectivity highlights its potential for precise mRNA delivery to specific immune cell subsets. Notably, the DOTMA-based formulation performed comparably to a commercially available product with an undisclosed composition. In contrast, while c-DOTAP exhibited a favorable safety profile, its

transfection efficiency was lower, underscoring DOTMA's superior functionality. These findings underscore the importance of optimizing both formulation and concentration for targeted transfection of immune cells, especially monocytes and macrophages, with potential applications in delivering immunomodulatory proteins.

However, certain limitations should be considered. The unknown composition of LipidFlex restricts direct comparisons and mechanistic insights. Additionally, while this study assessed in vitro transfection efficiency, further research is needed to evaluate in-vivo performance, biodistribution, and immunogenicity. Lastly, validating selective targeting in specific immune cell subsets remains crucial to confirming clinical relevance.

### **Declaration of competing interest**

The authors declare that they have no known competing financial interests or personal relationships that could have appeared to influence the work reported in this paper.

### Acknowledgments

This work was funded by the National Center for Gene Therapy and Drugs based on RNA Technology (www.rna-genetherapy.eu) Next Generation EU- (PNRR) - Mission 4 Component 2 Investment 1.4 - D.D. n. 3138 del 16/12/2021 and D.D. n. 3175 del 18/12/2021- Prot. CN00000041 - CUP: D43C22001200001 - Authorization n. 1035 del 17/06/2022 under the collaboration between Spoke 8: Platforms for RNA/DNA Delivery and Spoke 4: Metabolic and Cardiovascular Diseases.

### Data availability

Data will be made available on request.

### References

- Ay, C., Reinisch, A., 2024. Gene therapy: principles, challenges and use in clinical practice. Wien Klin Wochenschr. https://doi.org/10.1007/s00508-024-02368-8.
- Aydin, O., Kanarya, D., Yilmaz, U., Tunç, C.Ü., 2022. Determination of Optimum Ratio of Cationic Polymers and Small Interfering RNA with Agarose Gel Retardation Assay. In: Arechavala-Gomeza, V., Garanto, A. (Eds.), Antisense RNA Design, Delivery, and Analysis, Methods in Molecular Biology. Springer, US, New York, NY, pp. 117–128. https://doi.org/10.1007/978-1-0716-2010-6-7.
- Chen, Q., Wang, X., Zhang, Y., Tian, M., Duan, J., Zhang, Y., Yin, H., 2024. Minimizing the ratio of ionizable lipid in lipid nanoparticles for *in vivo* base editing. Natl. Sci. Rev. 11, nwae135. https://doi.org/10.1093/nsr/nwae135.
- Ciaglia, E., Montella, F., Trucillo, P., Ciardulli, M.C., Di Pietro, P., Amodio, G., Remondelli, P., Vecchione, C., Reverchon, E., Maffulli, N., Puca, A.A., Della Porta, G., 2019. A bioavailability study on microbeads and nanoliposomes fabricated by dense carbon dioxide technologies using human-primary monocytes and flow cytometry assay. Int. J. Pharm. 570, 118686. https://doi.org/10.1016/j. iipharm.2019.118686.
- Gimondi, S., Ferreira, H., Reis, R.L., Neves, N.M., 2023. Microfluidic Devices: A Tool for Nanoparticle Synthesis and Performance Evaluation. ACS Nano 17, 14205–14228. https://doi.org/10.1021/acsnano.3c01117.
- Giudice, V., Scala, P., Lamparelli, E.P., Gorrese, M., Serio, B., Bertolini, A., Picone, F., Della Porta, G., Selleri, C., 2024. Biomimetic Proteolipid Vesicles for Reverting GPI Deficiency in Paroxysmal Nocturnal Hemoglobinuria. iScience 27, 109021. https://doi.org/10.1016/j.isci.2024.109021.
- Guéguen, C., Ben Chimol, T., Briand, M., Renaud, K., Seiler, M., Ziesel, M., Erbacher, P., Hellal, M., 2024. Evaluating how cationic lipid affects mRNA-LNP physical properties and biodistribution. Eur. J. Pharm. Biopharm. 195, 114077. https://doi. org/10.1016/j.ejpb.2023.08.002.
- Jahn, A., Vreeland, W.N., Gaitan, M., Locascio, L.E., 2004. Controlled Vesicle Self-Assembly in Microfluidic Channels with Hydrodynamic Focusing. J. Am. Chem. Soc. 126, 2674–2675. https://doi.org/10.1021/ja0318030.
- Ji, A., Xu, M., Pan, Y., Diao, L., Ma, L., Qian, L., Cheng, J., Liu, M., 2023. Lipid Microparticles Show Similar Efficacy With Lipid Nanoparticles in Delivering mRNA and Preventing Cancer. Pharm Res 40, 265–279. https://doi.org/10.1007/s11095-022-03445-1.
- Korzun, T., Moses, A.S., Diba, P., Sattler, A.L., Taratula, O.R., Sahay, G., Taratula, O., Marks, D.L., 2023. From Bench to Bedside: Implications of Lipid Nanoparticle Carrier Reactogenicity for Advancing Nucleic Acid Therapeutics. Pharmaceuticals 16, 1088. https://doi.org/10.3390/ph16081088.
- Lamparelli, E.P., Marino, M., Scognamiglio, M.R., D'Auria, R., Santoro, A., Della Porta, G., 2024. PLA/PLGA nanocarriers fabricated by microfluidics-assisted

- nanoprecipitation and loaded with Rhodamine or gold can be efficiently used to track their cellular uptake and distribution. Int. J. Pharm. 667, 124934. https://doi.org/10.1016/j.ijpharm.2024.124934.
- Larson, N.R., Hu, G., Wei, Y., Tuesca, A.D., Forrest, M.L., Middaugh, C.R., 2022. pH-Dependent Phase Behavior and Stability of Cationic Lipid—mRNA Nanoparticles. J. Pharm. Sci. 111, 690–698. https://doi.org/10.1016/j.xphs.2021.11.004.
- Leung, A.K.K., Tam, Y.Y.C., Cullis, P.R., 2014. Lipid Nanoparticles for Short Interfering RNA Delivery, in: Advances in Genetics. Elsevier, pp. 71–110. https://doi.org/ 10.1016/B978-0-12-800148-6.00004-3.
- McKenzie, R.E., Minnell, J.J., Ganley, M., Painter, G.F., Draper, S.L., 2023. mRNA Synthesis and Encapsulation in Ionizable Lipid Nanoparticles. Current Protocols 3,
- Mehta, M., Bui, T.A., Yang, X., Aksoy, Y., Goldys, E.M., Deng, W., 2023. Lipid-Based Nanoparticles for Drug/Gene Delivery: An Overview of the Production Techniques and Difficulties Encountered in Their Industrial Development. ACS Mater Au 3, 600–619. https://doi.org/10.1021/acsmaterialsau.3c00032.
- Mehta, M.J., Kim, H.J., Lim, S.B., Naito, M., Miyata, K., 2024. Recent Progress in the Endosomal Escape Mechanism and Chemical Structures of Polycations for Nucleic Acid Delivery. Macromol. Biosci. 24, 2300366. https://doi.org/10.1002/ paghs/20236036
- Pfeifer, B.A., Beitelshees, M., Hill, A., Bassett, J., Jones, C.H., 2023. Harnessing synthetic biology for advancing RNA therapeutics and vaccine design. NPJ Syst Biol Appl 9, 60. https://doi.org/10.1038/s41540-023-00323-3.
- Qin, S., Tang, X., Chen, Y., Chen, K., Fan, N., Xiao, W., Zheng, Q., Li, G., Teng, Y., Wu, M., Song, X., 2022. mRNA-based therapeutics: powerful and versatile tools to combat diseases. Signal Transduct Target Ther 7, 166. https://doi.org/10.1038/s41392-022-01007-w.
- Roces, C.B., Lou, G., Jain, N., Abraham, S., Thomas, A., Halbert, G.W., Perrie, Y., 2020. Manufacturing Considerations for the Development of Lipid Nanoparticles Using Microfluidics. Pharmaceutics 12, 1095. https://doi.org/10.3390/ pharmaceutics12111095
- Santo, I.E., Campardelli, R., Albuquerque, E.C., De Melo, S.V., Della Porta, G., Reverchon, E., 2014. Liposomes preparation using a supercritical fluid assisted continuous process. Chem. Eng. J. 249, 153–159. https://doi.org/10.1016/j. cei.2014.03.099.
- Santo, I.E., Campardelli, R., Albuquerque, E.C., Vieira De Melo, S.A.B., Reverchon, E., Della Porta, G., 2015. Liposomes Size Engineering by Combination of Ethanol Injection and Supercritical Processing. J. Pharm. Sci. 104, 3842–3850. https://doi. org/10.1002/ips.24595.

- Schober, G.B., Story, S., Arya, D.P., 2024. A careful look at lipid nanoparticle characterization: analysis of benchmark formulations for encapsulation of RNA cargo size gradient. Sci Rep 14, 2403. https://doi.org/10.1038/s41598-024-52685-
- Sun, D., Lu, Z.-R., 2023. Structure and Function of Cationic and Ionizable Lipids for Nucleic Acid Delivery. Pharm Res 40, 27–46. https://doi.org/10.1007/s11095-022-03460-2
- Swetha, K., Kotla, N.G., Tunki, L., Jayaraj, A., Bhargava, S.K., Hu, H., Bonam, S.R., Kurapati, R., 2023. Recent Advances in the Lipid Nanoparticle-Mediated Delivery of mRNA Vaccines. Vaccines (basel) 11, 658. https://doi.org/10.3390/ vaccines.11030658
- Tang, X., Zhang, Y., Han, X., 2023. Ionizable Lipid Nanoparticles for mRNA Delivery. Advanced NanoBiomed Research 3, 2300006. https://doi.org/10.1002/anbr.202300006.
- Tenchov, R., Sasso, J.M., Zhou, Q.A., 2023. PEGylated Lipid Nanoparticle Formulations: Immunological Safety and Efficiency Perspective. Bioconjugate Chem. 34, 941–960. https://doi.org/10.1021/acs.bioconjchem.3c00174.
- Wong, W.D., Majnis, M.F., Lai, C.W., Sagadevan, S., Muhd Julkapli, N., 2024. Enhancement of mixing and reaction efficiency of various fluids applications at different microfluidic configuration and design. Chem. Eng. Process. - Process Intesif. 198, 109729. https://doi.org/10.1016/j.cep.2024.109729.
- Yan, J., Zhang, H., Li, G., Su, J., Wei, Y., Xu, C., 2024. Lipid nanovehicles overcome barriers to systemic RNA delivery: Lipid components, fabrication methods, and rational design. Acta Pharm Sin B 14, 579–601. https://doi.org/10.1016/j. apsb. 2023 10.012
- Yew, N.S., Scheule, R.K., 2005. Toxicity of Cationic Lipid-DNA Complexes, in: Advances in Genetics. Elsevier, pp. 189–214. https://doi.org/10.1016/S0065-2660(05)53007-4
- Yin, X., Harmancey, R., McPherson, D.D., Kim, H., Huang, S.-L., 2023. Liposome-Based Carriers for CRISPR Genome Editing. Int J Mol Sci 24, 12844. https://doi.org/ 10.3390/jims241612844.
- Yu, B., Lee, R.J., Lee, L.J., 2009. Microfluidic Methods for Production of Liposomes, in: Methods in Enzymology. Elsevier, pp. 129–141. https://doi.org/10.1016/S0076-6879(09)65007-2.
- Zhang, W., Jiang, Y., He, Y., Boucetta, H., Wu, J., Chen, Z., He, W., 2023. Lipid carriers for mRNA delivery. Acta Pharm. Sin. B 13, 4105–4126. https://doi.org/10.1016/j. apsb.2022.11.026.
- Zhang, Y., Gao, Z., Yang, X., Xu, Q., Lu, Y., 2024. Leveraging high-throughput screening technologies in targeted mRNA delivery. Mater. Today Bio 26, 101101. https://doi. org/10.1016/j.mtbio.2024.101101.